J. Opt. A: Pure Appl. Opt. **2** (2000) 481–487. Printed in the UK PII: S1464-4258(00)12721-7

Investigation of titanium- and copper-indiffused channel waveguides in lithium niobate and their application as holographic filters for infrared light

J Hukriede, D Kip and E Krätzig

Fachbereich Physik, Universität Osnabrück, D-49 069 Osnabrück, Germany

E-mail: joerg.hukriede@uos.de

Received 21 March 2000, in final form 12 July 2000

Abstract. Monomode channel waveguides for infrared light around 1550 nm are fabricated in lithium niobate by successive indiffusion of titanium stripes and thin evaporated layers of copper. The fabricated waveguides are optically characterized and investigated with an atomic force microscope. To evaluate the photorefractive properties holograms are recorded with green light of an argon ion laser and read in the various channels in reflection geometry with infrared light. The saturation values of the light-induced refractive-index change and the photoconductivity in the channels are measured. The results are consistent with a one-centre model for the charge transport. To demonstrate the multiplexing capabilities of the photorefractive waveguides three reflection holograms with 90% diffraction efficiency and a channel spacing of only 0.8 nm are superimposed in one sample.

Keywords: Integrated optics, holography, lithium niobate, multiplexer

1. Introduction

Lithium niobate ($LiNbO_3$) is a promising substrate material for applications in integrated optics because of its outstanding electro-optical and acousto-optical properties [1,2]. Channel waveguides are the basis for integrated circuits. Guides of high quality can be fabricated in $LiNbO_3$ by, e.g., indiffusion of thin evaporated or sputtered titanium (Ti) layers [3] or by proton exchange [4]. By these techniques devices such as directional couplers [5], fast light modulators [6] or complex integrated waveguide lasers [7] have been realized. Channel waveguides for infrared light around 1550 nm are of particular interest because in telecommunications more and more optical fibre systems are implemented. The fibres show their lowest loss in the region around 1550 nm. Monomode channel waveguides working in this wavelength range are easily produced in $LiNbO_3$ by suitable Ti indiffusion, i.e. appropriate tailoring of the channels' width and depth [8].

Furthermore, $LiNbO_3$ can be doped with various metal impurities to tailor its photorefractive properties for holography [9, 10]. The most commonly used dopants are iron and copper. $LiNbO_3$:Fe and $LiNbO_3$:Cu are sensitive to light in the visible green or blue wavelength region. Doped $LiNbO_3$ volume crystals are usually produced by adding CuO or Fe_2O_3 to the melt during crystal growth. Nevertheless, it is also possible to increase the impurity concentration of the material by indiffusion of thin evaporated layers at high temperatures. This technique is favourable for integrated optics because commercially available undoped $LiNbO_3$ wafers may be used. A desired region can be locally doped whereas the rest of the substrate remains unchanged. At high temperatures copper diffuses much more easily into $LiNbO_3$ than iron [11].

In this paper we investigate Ti-diffused monomode channel waveguides in $LiNbO_3$ for infrared light around 1550 nm additionally doped by copper indiffusion. To our knowledge only a few investigations in this particular field have been performed so far [12–14]. We present data regarding the optical quality of the guides for infrared light. The photorefractive properties of the waveguides are determined by recording reflection holograms with green light of an argon ion laser and diffracting the guided infrared light in the channels. It is shown that photorefractive $LiNbO_3$:Ti:Cu channel waveguides can serve as integrated narrow-bandwidth wavelength filters. They may be of potential use in the field of integrated optics, e.g. for integrated DBR waveguide lasers or WDM (wavelength division multiplexing) applications. In contrast to fibre Bragg gratings one may directly separate the diffracted light from the incoming light by utilizing a slanted Bragg grating in a planar waveguide geometry.

1464-4258/00/050481+07$30.00

2. Theory

To explain the process of hologram formation in $LiNbO_3$:Fe volume crystals the so-called 'one-centre model' was developed [15]. It also applies for $LiNbO_3$:Cu [16]. Copper was found to appear in two valence states, Cu^+ and Cu^{2+}. If the crystal is illuminated with a light intensity pattern in the photoactive green or blue wavelength region electrons are excited in the bright regions from Cu^+ ions which act as filled traps. The charge carriers are redistributed and finally trapped in the dark regions by Cu^{2+} ions. The bulk photovoltaic effect is the main charge driving force [17]. A space charge field builds up in the crystal and modulates the refractive index via the electro-optic effect.

The one-centre model predicts several linear relations involving the concentrations of filled and empty traps c_{Cu^+} and $c_{Cu^{2+}}$ if sufficient traps are present. The main outcomes are $\sigma_{ph} \propto (c_{Cu^+}/c_{Cu^{2+}})I$, $\Delta n_s \propto c_{Cu^{2+}}$ and $j_{phv} \propto c_{Cu^+}$. Here σ_{ph} is the photoconductivity, I the light intensity in the crystal, Δn_s the saturation value of the light-induced refractive-index modulation and j_{phv} the bulk photovoltaic current. The build-up of the refractive-index change Δn during hologram recording and its decay under homogeneous illumination follow exponential laws:

$$\text{recording: } \Delta n(t) = \Delta n_s(1 - \exp(-t/\tau)), \tag{1}$$

$$\text{erasure: } \Delta n(t) = \Delta n_0 \exp(-t/\tau), \tag{2}$$

$$\tau = \epsilon\epsilon_0/\sigma_{ph}. \tag{3}$$

Here t is the time, $\epsilon = 28$ is the appropriate dielectric constant [18] and ϵ_0 is the permittivity of free space.

Elementary holograms, sinusoidal refractive-index Bragg gratings, are recorded by superposition of two coherent plane waves. The diffraction efficiency η of an unslanted reflection grating depends on Δn and the read-out wavelength λ via the relation [19]

$$\eta = \left(1 + \frac{1 - \chi^2/\Phi^2}{\sinh^2\left(\Phi\sqrt{1 - \chi^2/\Phi^2}\right)}\right)^{-1}, \tag{4}$$

$$\Phi = \pi\,\Delta n\, d/\lambda, \qquad \chi = (\lambda - \lambda_p)\pi\, d/\lambda_p\Lambda. \tag{5}$$

Here d is the length of the grating and λ_p the peak wavelength where the Bragg condition is exactly matched. For $\lambda = \lambda_p$ equation (4) simplifies to

$$\eta(\lambda_p) = \tanh^2(\pi\,\Delta n\, d/\lambda_p). \tag{6}$$

Here $\eta(\lambda_p)$ is the maximum diffraction efficiency of the holographic grating.

3. Experimental methods

3.1. Waveguide fabrication

Our channel waveguides are fabricated in the following way: an undoped and polished y-cut $LiNbO_3$ wafer of congruently melting composition is cut into pieces of 7×17 mm^2, the c-axis of the crystals pointing along the larger side. An electron beam is used to deposit a 100 nm Ti layer on the top face of each sample. With the help of photolithography followed by a wet chemical etching process 6 and 8 μm wide Ti stripes are fabricated along the c-axis of the crystals. The channels are indiffused for 22 h at 1000 °C in air resulting in single-mode channel waveguides for infrared light around 1550 nm. During annealing the samples are wrapped in platinum foil. In the next step thin copper layers of various thicknesses τ_{Cu} (6, 19, 38, 57 and 83 nm) are deposited on the top face of the samples by thermal evaporation. The layers are indiffused for 2 h at a temperature of 1000 °C in a wet argon atmosphere to increase the number of photorefractive centres in the channels. With the help of the diffusion constants for copper [11] and Ti [20] in $LiNbO_3$ at 1000 °C the concentration profiles of the metals in the samples are calculated. Figure 1 shows the result for an 8 μm wide channel in waveguide 'K4' (57 nm Cu). Here the distribution $c_{Ti}(y)$ of Ti is a measure for the depth of the channel waveguide. As a result of the extremely different diffusion constants the copper doping level in the channel is nearly constant. In the first 10 μm $c_{Cu}(y)$ varies by less than 0.5%. In the following the term c_{Cu} always refers to the copper concentration in the channels. The fabrication parameters of the investigated channel waveguides are summarized in table 1.

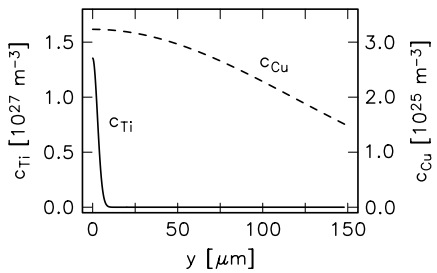

Figure 1. Calculated Ti and copper concentrations c_{Ti} and c_{Cu} versus crystal depth y for the waveguide 'K4' (57 nm Cu) in the middle of the 8 μm wide channel. The copper concentration is almost constant in the waveguide layer.

Table 1. Fabrication parameters of the investigated waveguides. Here τ_{Cu} is the thickness of the evaporated copper layer, c_{Cu} the copper concentration in the channels and l the length of the waveguide.

Sample	τ_{Cu} (nm)	c_{Cu}(10^{25} m^{-3})	l (mm)
U3	—	—	16.0
K1	6	0.4	15.0
K3	19	1.1	14.0
K5	38	2.2	15.0
V2	38	2.2	3.0
K4	57	3.2	16.0
S4, S6	83	4.7	16.0
U4	83	4.7	1.2

3.2. Investigation of surface profiles

The surface profiles of the fabricated waveguides are investigated with an atomic force microscope (AFM) in the contact mode. Here the 8 μm wide channels are scanned along the z-direction and height topographies of the surface planes are taken. The flatness of the channels is characterized

by calculating the corresponding roughness parameter R_a. Here the height profile of a single line along the channel is taken out of the surface topography. The roughness of this line is defined as

$$R_a = \frac{1}{n_0} \sum_{n=1}^{n_0} \Delta y(z_n), \tag{7}$$

where $\Delta y(z_n)$ denotes the positive height deviation from the average height of the extracted line at the coordinate z_n and n_0 the total number of data points analysed.

3.3. Endface coupling and waveguide losses

All waveguides are investigated with infrared probe light supplied by a DFB laser with optical fibre output. The laser is tunable between 1555.4 and 1559.4 nm in steps of 0.01 nm. The linewidth of the laser is smaller than 1×10^{-4} nm. The light is directed through an optical fibre isolator to prevent back-reflections. A 3 dB coupler is appended to monitor the laser power. Finally, a fibre polarizer is inserted to control the polarization state of the infrared light. This allows us to excite either the TE or the TM mode in the channel waveguide. The light is coupled into and out of the investigated channel by direct fibre-to-channel coupling via the precisely polished endfaces. Here the bare ends of the in- and outcoupling fibre are mounted on precise piezo-driven xyz-translation stages that allow us to adjust the fibres' positions with an absolute accuracy better than 30 nm. The outcoupled light is directed onto a germanium photodetector to measure the intensity. It is normalized to the initial laser power measured with the 3 dB coupler. Each waveguide endface is anti-reflection coated for the transition between $LiNbO_3$ and air by evaporation of a single layer of 290 nm MgF_2. The bottom faces of the samples are anti-reflection coated for the green recording light with a layer of 110 nm MgF_2. The deposition of MgF_2 allows us to keep the samples at room temperature during evaporation.

The loss of light intensity during a transition from the fibre to the channel is estimated in the following way: the overlap integral ρ between the field distribution F_f in the fibre and the field F_{ch} in the channel is calculated numerically via the formula

$$\rho = \frac{|\iint F_f\, F_{ch}\, dx\, dy|^2}{\iint |F_{ch}|^2\, dx\, dy \times \iint |F_f|^2\, dx\, dy}. \tag{8}$$

For the prepared waveguides we obtain a value of typically $\rho = 90\%$. Fresnel reflections occur at the transition between fibre and air. Their amount is about 4%. To take into account imperfect polishing/cleaning of the endfaces of waveguide and fibre an additional loss of 5% is estimated. This means that approximately 18% of intensity is lost at a transition from fibre to channel. The losses α in the channel itself are calculated by the relation $\alpha = -1/l \times \ln(I_{out}/I_{in})$ where l is the waveguide length, I_{in} the light intensity at $z = 0$ and I_{out} the intensity at $z = l$.

3.4. Holographic experiments

Refractive-index gratings are recorded in the samples utilizing a two-beam holographic setup with active stabilization [21]. The recording and read-out geometry is illustrated in figure 2. Green light from an argon ion laser at a wavelength of $\lambda_w = 514$ nm is split into two coherent, ordinarily polarized beams. The first one is spatially filtered and expanded and impinges upon the sample as a plane wave. The sample is mounted onto a precise rotary table and can be turned around the x-direction. The second beam is launched into a polarization preserving single-mode fibre. The fibre end is mounted onto a second rotary table together with a collimating system. The rotation axes of the two tables coincide. The beam also hits the sample and an interference pattern is formed on the top face. The light intensity of each recording beam is 600 W m^{-2}. The grating period is

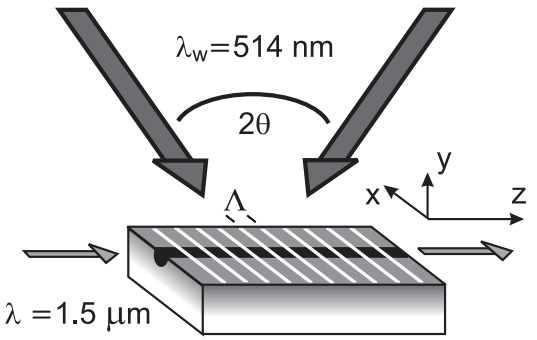

Figure 2. Scheme of the recording and readout geometry for the holographic measurements. The gratings recorded with green light form reflection holograms for the infrared readout light in the channels.

$$\Lambda = \lambda_w/(2 \sin \Theta) \tag{9}$$

where 2Θ is the intersecting angle of the two beams in air. The grating vector is directed along the z-direction, parallel to the channels. The angle mismatch between grating vector and channel in the xz-plane is less than 0.3°. The holograms are read in reflection geometry in the channels with guided infrared light of the TM mode. Here the wavelength of the DFB laser is tuned and the normalized transmission characteristic $T(\lambda)$ of the channel is measured. At the peak wavelength λ_p the Bragg condition for readout

$$\Lambda = \lambda_p/2n_{eff} \tag{10}$$

is exactly matched. Here n_{eff} is the effective refractive index of the guided mode. The transmission T drops down from unity to a minimum. The diffraction efficiency of the holographic grating is given by $\eta = 1 - T(\lambda_p)$.

The photoconductivity σ_{ph} in the channels is evaluated by measuring the decay of a holographic grating under homogeneous illumination with photoactive light. Transmission spectra $T(\lambda)$ are taken permanently while an expanded green beam of the argon ion laser impinges on the top face of the waveguide.

The effective refractive indices n_{eff} of the channel waveguides are determined by recording a reflection grating and measuring the resulting peak wavelength λ_p for the infrared light. By combining equations (9) and (10) one obtains the relation $n_{eff} = \lambda_p \sin(\Theta)/\lambda_w$.

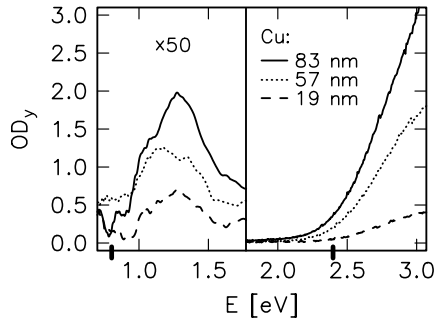

Figure 3. Optical density OD_y of the samples along the y-direction versus energy E of the probe light.

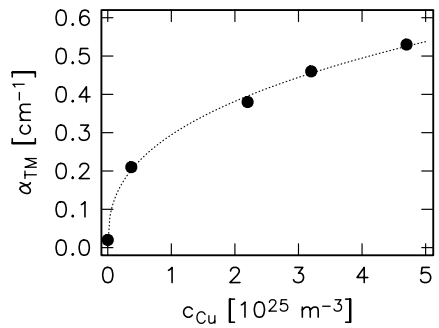

Figure 4. Waveguide losses α_{TM} of 6 μm wide channels versus copper concentration c_{Cu}. The probe light is TM polarized and has a wavelength of $\lambda = 1555.4$ nm. The dotted line is a guide for the eye.

4. Experimental results

4.1. Waveguide losses and waveguide quality

Figure 3 shows measurements of the optical density OD_y of some of the prepared samples versus the probe light energy E taken with a CARY 17D spectrometer. In each case the corresponding curve for an undoped sample has been subtracted. The light impinges upon the crystals along the y-direction, perpendicular to the channel waveguides. The energy of the green light of the argon ion laser at 2.4 eV and the energy of the infrared light emitted by the DFB laser at 0.8 eV are marked on the energy scale. The left part of the diagram is magnified 50-fold. The measured spectra look very similar to those of conventionally fabricated $LiNbO_3$:Cu volume crystals doped in the melt [16]: the shoulder starting at approximately 2 eV is related to an electronic transition from the Cu^+ level into the conduction band. The small band at 1.2 eV originates from a crystal field transition involving the Cu^{2+} state. Both characteristics become more pronounced with increasing copper concentration. In particular the shoulder beginning at 2 eV rises dramatically. For infrared light around 1550 nm no clear tendency is observed. In this range we measure $OD_y \leqslant 0.01$ for all samples. It is not appropriate to calculate absorption spectra $\alpha(E)$ from $OD_y(E)$ because the copper concentration is inhomogeneous along the y-direction.

Figure 4 presents direct measurements of the waveguide losses α_{TM} at a wavelength of 1555.4 nm versus copper concentration c_{Cu}. Here the 6 μm wide channels are investigated. The losses of the waveguides strongly depend on c_{Cu}. The undoped sample investigated for comparison shows by far the lowest loss. Here we find a value of $\alpha_{TM} = 0.02$ cm^{-1}, which is equal to a loss of only 0.09 dB cm^{-1}. For the highest doping level we measure $\alpha_{TM} = 0.53$ cm^{-1}, which corresponds to 2.30 dB cm^{-1}.

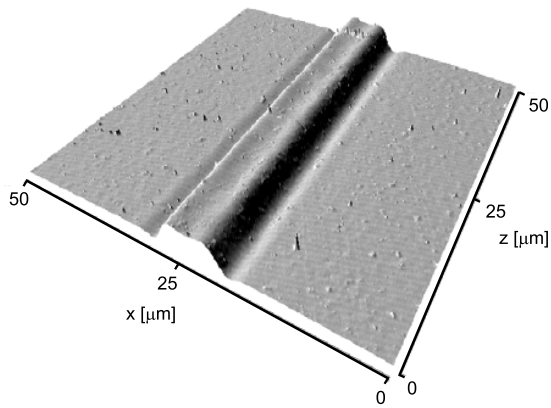

Figure 5. Surface profile of the sample 'K3' (19 nm Cu) measured with an AFM. The 8 μm wide channel is shown.

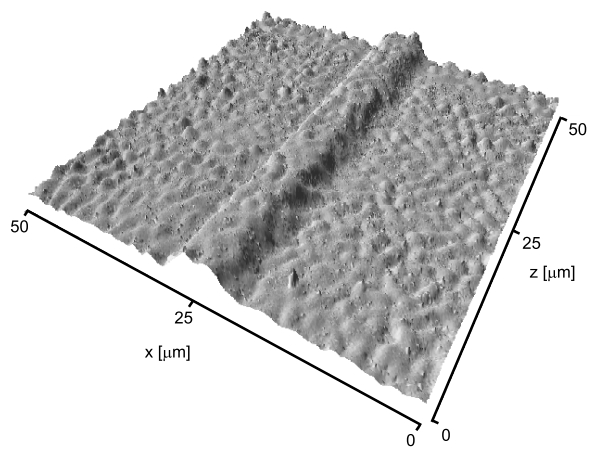

Figure 6. Surface profile of the sample 'S4' (83 nm Cu) measured with the AFM. Again the 8 μm wide channel is shown.

To examine the surface quality of the fabricated waveguides AFM measurements are performed. The reconstructed surface topographies extend over an area of 50×50 μm^2. The results are shown in figure 5 for waveguide 'K3' (19 nm Cu) and in figure 6 for waveguide 'S4' (83 nm Cu). For both samples an 8 μm wide channel is investigated. The surface of sample 'K3' looks similar to that of the undoped sample 'U3'. Both are flat and smooth. On the other hand the surface of sample 'S4' is very rough. During indiffusion the channels expand out of the surface by approximately 200 nm. A height measurement for sample 'K3' along the x-direction is presented in figure 7.

To quantify the surface quality of the channels we evaluate the various surface topographies in the region of the indiffused Ti along the z-direction. From these data the roughness of each channel is calculated via equation (7). The roughness parameter R_a is plotted versus copper concentration in figure 8. For an evaporated copper layer up to 38 nm the surface quality is still close to that of the undoped channel waveguide 'U3'. For a larger thickness R_a increases rapidly.

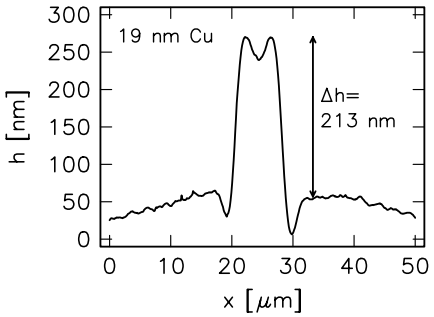

Figure 7. Height profile h along the x-direction of an 8 μm wide channel in the sample 'K3' (19 nm Cu) measured with the AFM. Here the coordinate z is kept constant.

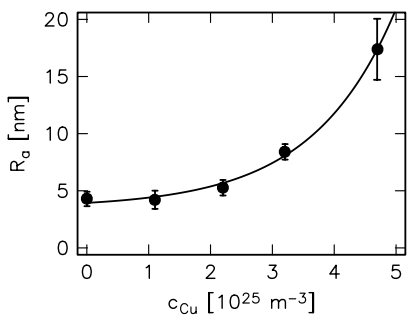

Figure 8. Roughness parameter R_a of the channel waveguides versus copper concentration c_{Cu}. Here the surface relief of the channels along the z-direction is investigated for constant x. The interpolated curve is a guide for the eye.

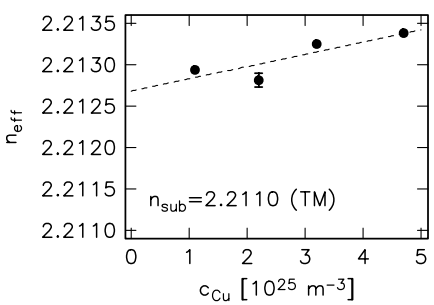

Figure 9. Effective refractive index n_{eff} of the TM mode in an 8 μm wide channel extracted from the holographic measurements versus copper concentration c_{Cu} in the channels. The dashed line is a linear fit.

The fabrication of an infrared wavelength filter [22–24] operating at a predefined peak wavelength λ_p requires the knowledge of the effective refractive index n_{eff} of the guide. Then the appropriate recording angle is given by equations (9) and (10). The measured values n_{eff} for the 8 μm wide channel waveguides are presented in figure 9 versus copper concentration c_{Cu}. In each case the TM mode is excited. A slight increase of n_{eff} is observed for large copper doping levels. The corresponding substrate refractive index is $n_{sub} = 2.2110$ (see below).

4.2. Photorefractive properties

In the next step we investigate the fundamental photorefractive properties of the fabricated guides. The saturation values Δn_s of the optically induced refractive-index modulation

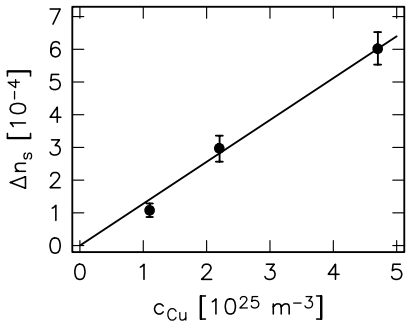

Figure 10. Saturation values Δn_s of the refractive-index modulation induced by the green recording light in the channel waveguides versus copper concentration c_{Cu}. The solid line is a linear fit.

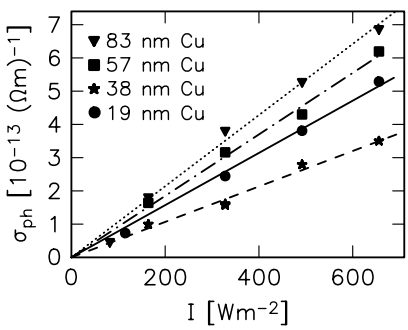

Figure 11. Photoconductivity σ_{ph} of some investigated channel waveguides versus intensity I of the green erasure light. The lines are linear fits.

in the channels are extracted from time dependent measurements: reflection holograms are written in each sample for different recording times t. The evolution of the obtained values $\Delta n(t)$ follows the relation (1) predicted by the one-centre model. A computer fit for each sample yields the saturation values Δn_s. The measured data for three investigated samples are shown in figure 10 versus copper concentration in the channels. The solid line is a linear fit.

The photoconductivity σ_{ph} is determined by measuring the decay of recorded reflection holograms under homogeneous illumination with green light. Here, all measured curves for $\Delta n(t)$ are well fitted by single-exponential decay curves according to equation (2). The extracted values for σ_{ph} of some selected samples are plotted in figure 11 versus intensity I of the green erasure light in the crystal. Each data set is described well by a linear fit.

To demonstrate the multiplexing capabilities of the fabricated channel waveguides three reflection holograms with a peak spacing of only 0.8 nm are superimposed in sample 'S6' (83 nm Cu). The holograms are recorded one after the other; the exposure times and recording angles are $t = 16$ min and $2\Theta = 93.87^\circ$ for grating (a), $t = 4$ min and $2\Theta = 93.93^\circ$ for grating (b) and $t = 1.5$ min and $2\Theta = 93.99^\circ$ for grating (c). The resulting transmission spectrum $T(\lambda)$ of the channel waveguide for the TM mode is plotted in figure 12. The measured diffraction efficiencies of the three gratings are 84.9, 96.7 and 95.2%. The peak wavelengths λ_p are 1558.29, 1557.50 and 1556.68 nm. A crucial characteristic of these reflection gratings is the minimum peak width $\Delta\lambda$ that can be obtained. A common measure is the half width FWHM

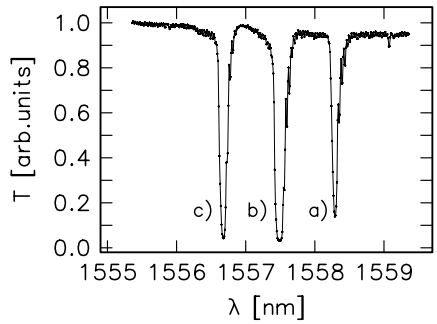

Figure 12. Three superimposed reflection holograms for infrared light in an 8 μm wide channel in sample 'S6' (83 nm Cu). The normalized transmission T of the waveguide is shown versus the readout wavelength λ. A hologram spacing of 0.8 nm is realized.

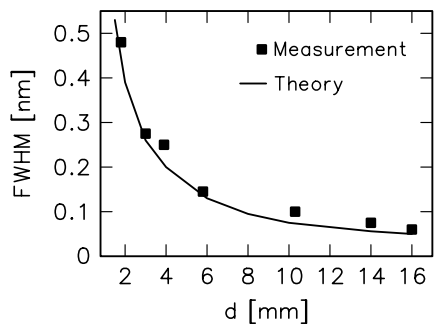

Figure 13. Peak width FWHM of reflection gratings versus grating length d for holograms recorded in waveguide 'S6' (squares) and theoretical values (solid curve).

(full width at half minimum). The peak widths of the three gratings are 0.12, 0.15 and 0.09 nm, respectively.

The experimental and the theoretical dependence of the FWHM on the total grating length d for a grating of $\eta = 80\%$ strength is presented in figure 13. The squares represent data measured with waveguide 'S6' and the solid curve was calculated according to equation (4). Here the different grating lengths are experimentally realized by applying an appropriate slit on top of the sample during hologram recording. Theory and experiment fit together very well. The minimum experimentally realized FWHM is 0.07 nm for a 16 mm long grating. For a grating length of 1.8 mm the FWHM obtained by experiment increases to 0.48 nm.

A holographic grating written at room temperature is not stable enough for most applications. The dark conductivity in our channel waveguides is not negligible and we observe a slow decay of the diffraction efficiency of the recorded holograms. The decay time is in the range of several weeks. Nevertheless, the technique of thermal fixing [25–27] yields quasi-permanent holograms. Here the gratings have to be recorded at elevated temperatures around 180 °C. Thermal fixing works in our waveguides, too. We will report on this field in a different contribution [28].

5. Discussion

5.1. Waveguide losses and optical density

The increased losses of the copper-doped channel waveguides around 1550 nm are caused by two effects. Figure 8 indicates that the surface roughness rises dramatically for high copper doping levels in the channels. This may originate from an increased outdiffusion of lithium [29] during the indiffusion of thick layers of copper. This means that for these samples light is lost due to strong scattering through the channel surface. Absorption of the infrared light in the channels resulting from the presence of Cu^{2+} has to be taken into account, too. The strong increase of the waveguide loss α_{TM} even for a low copper doping level (figure 4) is an indication for this. Here the surface roughness R_a of the channels is still almost equal to that of the undoped sample (figure 8). On the other hand, no clear influence of the rising Cu^{2+} band on infrared light absorption around 1550 nm is estimated from the optical density measurements in figure 3. This may result from the fact that for light travelling along the y-direction the copper layer is too thin to produce a pronounced effect, in contrast to the guided TM mode propagating in the channel. We are confident that the losses of the waveguides can be significantly decreased if the copper indiffusion is performed in a highly reducing environment, e.g. in vacuum atmosphere. This lowers the number of Cu^{2+} centres in the channels and consequently the absorption band at 1.2 eV.

5.2. Holographic measurements

Figure 9 indicates that the effective refractive indices of the TM mode in the investigated 8 μm wide channel waveguides are all between $n_{eff} = 2.2127$ and 2.2134. Obviously, the refractive index of the substrate material must be below these values. An interpolation of data from [30] yields the ordinary refractive index of undoped $LiNbO_3$ at 1557 nm. We obtain $n_o = 2.2110$. This means that for the guided TM mode the refractive-index increase induced by the indiffused Ti is about 2×10^{-3}.

An additional small increase of n_{eff} appears for large copper doping levels. As c_{Cu} is practically constant in the channels (figure 1), this suggests that the indiffused copper has slightly enhanced the refractive index n_o of the substrate. However, this increase induced by the presence of copper is small compared to the influence of the indiffused Ti. It might already be in a range where unavoidable tolerances during waveguide fabrication can significantly affect the results.

We also image the intensity distribution at the rear endface of the channel waveguides onto an infrared camera to check whether the indiffused copper induces an additional planar waveguide at the surface of the doped region of the samples: this is not the case. Even for the highest copper doping level no guided light is observed to the left or right of the Ti indiffused channels. This holds for both polarization states of the infrared light.

Figure 11 shows that for all investigated waveguides the photoconductivity rises linearly with light intensity as predicted by the one-centre model. Thus only the copper impurities are responsible for the photorefractive effect in the waveguides: no influence of the Ti ions defining the channels is observed. No obvious relation between the slope $\sigma_{ph,0} \equiv \sigma_{ph}/I$ and c_{Cu} is observed. The values for $\sigma_{ph,0}$ extend from 5.3×10^{-16} to 10.7×10^{-16} mV^{-2}. This is in very good agreement with data obtained for homogeneously doped volume crystals containing the same amount of copper [31].

The second prediction, $\Delta n_s \propto c_{Cu^{2+}}$, cannot be checked because the total Cu^{2+} content in the channels is unknown. If we assume that the reduction state $c_{Cu^+}/c_{Cu^{2+}}$ of the investigated samples does not differ too much (the annealing treatment is the same for all crystals) Δn_s should also increase linearly with the total copper concentration c_{Cu}. This linear dependence is observed in figure 10. The maximum values obtained for Δn_s coincide with those of highly copper- or iron-doped $LiNbO_3$ volume crystals [31, 32].

For applications such as wavelength filtering a high diffraction efficiency is required. From equation (6) one obtains that for a 16 mm long grating a refractive-index modulation of $\Delta n = 1.3 \times 10^{-4}$ yields a theoretical diffraction efficiency of $\eta = 99.9\%$ for the infrared light. This is equal to a rejection ratio of 30 dB for the peak wavelength λ_p. Figure 10 shows that this can already be reached with a moderate copper doping level.

6. Conclusions

In summary, we have reported on the investigation of photorefractive monomode channel waveguides in lithium niobate fabricated by Ti and additional copper indiffusion. The waveguide losses for infrared light around 1550 nm strongly depend on the copper impurity level in the channels. The fundamental photorefractive properties of the waveguides are comparable to those of conventionally doped $LiNbO_3$:Cu volume crystals. They are in accordance with the predictions of a one-centre model for the charge transport. Infrared light can be efficiently diffracted from recorded reflection gratings, which allows us to fabricate an integrated narrow-bandwidth filter.

Acknowledgment

Financial support of the Deutsche Forschungsgemeinschaft (grant SFB 225, D9) is gratefully acknowledged.

References

[1] Tamir T (ed) 1990 *Guided-Wave Optoelectronics* (Berlin: Springer)
[2] Prokhorov A M, Kuzminov Y S and Khachaturyan O A 1996 *Ferroelectric Thin-Film Waveguides in Integrated Optics* (Cambridge: Cambridge International Science)
[3] Schmidt R V and Kaminov I P 1974 Metal-diffused optical waveguides in $LiNbO_3$ *Appl. Phys. Lett.* **25** 458–60
[4] Jackel J L, Rice C E and Veselka J J 1983 Proton exchange in $LiNbO_3$ *Ferroelectrics* **50** 165–70
[5] Alferness R C, Schmidt R V and Turner E H 1979 Characteristics of Ti-diffused lithium niobate optical directional couplers *Appl. Opt.* **18** 4012–6
[6] Burns W K, Lee A B and Milton A F 1976 Active branching waveguide modulator *Appl. Phys. Lett.* **29** 790–2
[7] Becker C, Greiner A, Oesselke T, Pape A, Sohler W and Suche H 1998 Integrated optical Ti:Er:$LiNbO_3$ distributed Bragg reflector laser with a fixed photorefractive grating *Opt. Lett.* **15** 1194–6
[8] Zhang D, Ding G and Chen C 1998 Theoretical analysis of guided mode and effective refractive index at 1.53 μm in Ti:$LiNbO_3$ strip waveguides *J. Lightwave Technol.* **16** 459–64
[9] Chen F S, LaMacchia J T and Fraser D B 1968 Holographic storage in lithium niobate *Appl. Phys. Lett.* **13** 223–5
[10] Ashkin A, Boyd G D, Dziedzic J M, Smith R G, Ballman A A, Levinstein J J and Nassau K 1966 Optically-induced refractive index inhomogeneities in $LiNbO_3$ and $LiTaO_3$ *Appl. Phys. Lett.* **9** 72–4
[11] Hukriede J, Kip D and Krätzig E 1999 Copper diffusion into lithium niobate *Phys. Status Solidi* a **172** R3
[12] Popov V L and Shandarov V M 1991 Study of planar waveguides fabricated from lithium niobate by successive diffusion of titanium and copper *Sov. Phys.–Tech. Phys.* **36** 1380–2
[13] Mikami O 1976 Electro-optic light modulation with holographic gratings stored in a Cu-diffused $LiNbO_3$ plate *Opt. Commun.* **19** 42–4
[14] Bozhevol'nyi S I, Zolotov E M, Kiselev V A and Sherbakov E A 1979 Investigation of diffraction gratings induced in $LiNbO_3$ for integrated-optics applications *Sov. J. Quantum Electron.* **9** 216–8
[15] Kurz H, Krätzig E, Keune W, Engelmann H, Gonser U, Dischler B and Räuber A 1977 Photorefractive centers in $LiNbO_3$ studied by optical-, Mössbauer-, and EPR-methods *Appl. Phys.* **12** 355–68
[16] Krätzig E and Orlowski R 1980 Light induced charge transport in doped $LiNbO_3$ and $LiTaO_3$ *Ferroelectrics* **27** 241–4
[17] Glass A M, von der Linde D and Negran T J 1974 High-voltage bulk photovoltaic effect and the photorefractive process in $LiNbO_3$ *Appl. Phys. Lett.* **25** 233–5
[18] Mansingh A and Dhar A 1985 The AC conductivity and dielectric constant of lithium niobate single crystals *J. Phys. D: Appl. Phys.* **18** 2059–71
[19] Kogelnik H 1969 Coupled wave theory for thick hologram gratings *Bell Syst. Tech. J.* **48** 2909–47
[20] Kip D, Gather B, Bendig H and Krätzig E 1993 Concentration and refractive index profiles of titanium- and iron-diffused planar $LiNbO_3$ waveguides *Phys. Status Solidi* a **139** 241–8
[21] Freschi A A and Frejlich J 1995 Adjustable phase control in stabilized interferometry *Opt. Lett.* **20** 635–7
[22] Leyva V, Rakuljic G A and O'Conner B 1994 Narrow bandwidth volume holographic optical filter operating at the Kr transition at 1547.82 nm *Appl. Phys. Lett.* **65** 1079–81
[23] Müller R, Alvarez-Bravo J V, Arizmendi L and Cabrera J M 1994 Tuning of photorefractive interference filters in $LiNbO_3$ *J. Phys. D: Appl. Phys.* **27** 1628–32
[24] Hukriede J, Kip D and Krätzig E 1998 Thermally fixed reflection gratings for infrared light in $LiNbO_3$:Ti:Fe channel waveguides *Opt. Lett.* **23** 1405–7
[25] Amodei J J and Staebler D L 1971 Holographic pattern fixing in electro-optic crystals *Appl. Phys. Lett.* **18** 540–4
[26] Buse K, Breer S, Peithmann K, Kapphan S, Gao M and Krätzig E 1997 Origin of thermal fixing in photorefractive $LiNbO_3$ crystals *Phys. Rev.* B **56** 1225–35
[27] An X, Psaltis D and Burr G W 1999 Thermal fixing of 10 000 holograms in $LiNbO_3$:Fe *Appl. Opt.* **38** 386–93
[28] Hukriede J, Kip D and Krätzig E 2000 Permanent reflection holograms for infrared light recorded in $LiNbO_3$:Ti:Cu channel waveguides at press
[29] Kaminow I P and Carruthers J R 1973 Optical waveguiding layers in $LiNbO_3$ and $LiTaO_3$ *Appl. Phys. Lett.* **22** 326–8
[30] Nelson D F and Mikulyak R M 1974 Refractive indices of congruently melting lithium niobate *J. Appl. Phys.* **45** 3688–9
[31] Peithmann K, Hukriede J, Buse K and Krätzig E 2000 Photorefractive properties of lithium niobate volume crystals doped by copper diffusion *Phys. Rev.* B **61** 4615–20
[32] Peithmann K, Wiebrock A and Buse K 1999 Photorefractive properties of highly doped lithium niobate crystals in the visible and near-infrared *Appl. Phys.* B **68** 777–84